

Article

Tsallis Holographic Dark Energy with Power Law Ansatz Approach

Oem Trivedi ^{1,*}, Maxim Khlopov ^{2,3,4,†} and Alexander V. Timoshkin ^{5,6,†}

- ¹ International Centre for Space and Cosmology, School of Arts and Sciences, Ahmedabad University, Ahmedabad 380009, India
- ² Research Institute of Physics, Southern Federal University, 344090 Rostov-on-Don, Russia; khlopov@apc.in2p3.fr
- ³ Virtual Institute of Astroparticle Physics, 75018 Paris, France
- ⁴ Center for Cosmoparticle Physics Cosmion, National Research Nuclear University “MEPHI”, 115409 Moscow, Russia
- ⁵ Institute of Scientific Research and Development, Tomsk State Pedagogical University (TSPU), 634061 Tomsk, Russia; alex.timosh@rambler.ru
- ⁶ Laboratory of Theoretical Cosmology, International Centre of Gravity and Cosmos, Tomsk State University of Control Systems and Radio Electronics (TUSUR), 634050 Tomsk, Russia
- * Correspondence: oem.t@ahduni.edu.in
- † These authors contributed equally to this work.

Abstract: Holographic principles have proven to be a very interesting approach towards dealing with the issues of the late-time acceleration of the universe, which has resulted in a great amount of work on holographic dark energy models. We consider one such very interesting holographic scenario, namely the Tsallis Holographic dark energy model, and consider an ansatz based approach to such models. We consider three cosmological scenarios in such models, namely those with viscous, non-viscous, and Chaplygin gas scenarios, discussing various crucial aspects related to these models. We discuss various crucial properties of the Tsallis model in such scenarios and see how the phantom divide is crossed in each case, but it is only the Chaplygin gas models which provide a better view on stability issues. The symmetry property of the theory presented in the article is the assumption that space is isotropic. Using bulk viscosity instead of shear viscosity reflects spatial isotropy.

Keywords: holographic dark energy; chaplygin gas cosmology; viscous cosmology



Citation: Trivedi, O.; Khlopov, M.; Timoshkin, A.V. Tsallis Holographic Dark Energy with Power Law Ansatz Approach. *Symmetry* **2024**, *16*, 446. <https://doi.org/10.3390/sym16040446>

Academic Editor: Kazuharu Bamba

Received: 2 March 2024

Revised: 30 March 2024

Accepted: 1 April 2024

Published: 7 April 2024



Copyright: © 2024 by the authors. Licensee MDPI, Basel, Switzerland. This article is an open access article distributed under the terms and conditions of the Creative Commons Attribution (CC BY) license (<https://creativecommons.org/licenses/by/4.0/>).

1. Introduction

The surprising revelation of the late-time acceleration of the universe startled the cosmology community [1]. Subsequent efforts have been extensive in elucidating this expansion phenomenon. Numerous approaches have been pursued, encompassing traditional avenues like the cosmological constant [2–4], as well as unconventional theories such as modified gravity [5–7] and models involving scalar fields driving late-time cosmic acceleration [8–14]. Additionally, diverse perspectives within quantum gravity have contributed to addressing the cosmic acceleration enigma, ranging from braneworld cosmology in string theory to theories like loop quantum cosmology and asymptotically safe cosmology [15–27]. Nevertheless, these endeavors have underscored certain discrepancies, notably the Hubble tension, which refers to disparities in the values of the Hubble constant derived from detailed CMB maps, combined with baryon acoustic oscillations data and supernovae type Ia (SNeIa) data [28–30]. Consequently, the current epoch of the universe presents a myriad of inquiries and appears poised to evolve into a domain where advanced gravitational physics will illuminate a deeper comprehension of cosmology.

Among the various proposed solutions addressing the dark energy problem, one noteworthy proposition is the holographic principle [31,32], which carries significance within the realm of quantum gravity. At its core, the holographic principle posits that

a system's entropy is not dictated by its volume but rather by its surface area [33]. Cohen et al. [34], drawing from this principle, proposed a linkage between short-distance and long-distance cutoffs in quantum field theory, attributing it to the constraints imposed by black hole formation. In essence, if ρ denotes the quantum zero-point energy density due to a short-distance cutoff, the energy within a region of size L should not surpass the mass of a black hole of equivalent size, leading to the inequality $L^3\rho \leq LM_p^2$. The maximum permissible value for the infrared cutoff (L_{IR}) precisely satisfies this inequality, yielding the relationship:

$$\rho = 3M_p^2 c^2 L_{IR}^{-2}, \quad (1)$$

where c represents an arbitrary parameter, and M_p signifies the reduced Planck mass.

The holographic principle has found extensive application in cosmology, particularly in elucidating the late-time dark energy era, commonly known as holographic dark energy (HDE) (for a comprehensive review, refer to [35]). In this framework, the infrared cutoff, L_{IR} , originates from cosmological considerations. Nojiri et al. [36–39] introduced the most general form of this cutoff, termed the generalized HDE, which encompasses various combinations of the FRW parameters including the Hubble constant, particle and future horizons, cosmological constant, and the finite lifetime of the universe. Numerous other studies have investigated holographic dark energy from diverse perspectives in recent years [35,37,40–70]. In the present work, we want to discuss the properties of the Tsallis HDE model in a scale factor ansatz-based approach, which has been quite heavily discussed in recent times [71–74]. A scale factor ansatz approach to HDE scenarios, or even to study various late-time or even certain early-time scenarios, is quite a prevalent one as it allows one to, for example, reconstruct potentials etc. for viable cosmological evolutions. The mathematical formulation is quite straightforward, where one assumes an ansatz for the scale factor here and then sees how the other cosmologically relevant parameters turn out and whether the particular model at hand would allow for such an evolution while maintaining self consistency. This is what we have pursued, also by considering the Tsallis scenario in such a case. In the next section, we shall give a brief overview of the cosmological settings in which we would like to study our HDE scenario, discussing the non-viscous, viscous, and Chaplygin gas EOS in detail and their implications for the evolution of the universe. In Section 3, we discuss the important aspects of the models we are considering and see which of these can be best placed in the face of the usual issues faced by holographic models. We conclude our work in Section 4.

2. Tsallis Holographic Dark Energy and the Various EOS

Various interesting approaches towards holographic dark energy have been discussed in recent times. For example, [75] discussed the implications of quantum-gravitational effects on the entropy of black holes, even incorporating certain fractal behaviour as well. This led to the creation of the Barrow HDE model as well, where the DE energy density depends on the deformation parameter in the Barrow entropy. Similarly, Sheikahmadi's work [76] examines entropy bounds from lattice field theory and its implications for holographic dark energy. It very interestingly built upon this work to also show that the corrections to the electron magnetic momentum are of the order of $\mathcal{O}(10^{-23})$. Another very intriguing proposition within the realm of holographic dark energy is the Tsallis holographic dark energy model, often abbreviated as THDE. Tsallis and Cirto [77] introduced a generalized form of entropy, famously known as Tsallis entropy, to address thermodynamic inconsistencies in non-standard systems, such as black holes. The pioneering investigations into dark energy models using Tsallis' non-extensive statistical framework can be traced back to [78], with further explorations in cosmology detailed in [79]. This type of entropy aligns well with the Friedmann equations and Padmanabhan's proposal regarding the emergence of spacetime [80].

Similar to the conventional HDE model, it is feasible to formulate dark energy models utilizing Tsallis entropy. As a result, Tsallis holographic dark energy (THDE), using the Hubble horizon as an infrared (IR) cutoff, was introduced in [81]. Building upon this foun-

dation, the dynamics of Friedmann–Robertson–Walker (FRW) universes, considering dark matter and THDE with various IR cutoffs such as the apparent horizon, the particle horizon, the Ricci scalar curvature scale, and the Granda–Oliveros (GO) scale, were examined in non-interacting and interacting scenarios [82–85].

It was found that the THDE model with the particle horizon as the IR cutoff provides an explanation for the ongoing accelerated expansion of the universe, unlike the corresponding conventional HDE model. The findings presented in [82] indicate that the stability of the THDE model varies depending on the choice of the GO scale and the Ricci scalar cutoff, in both interacting and non-interacting scenarios. However, in [83], it is demonstrated that the THDE model with the GO scale as the IR cutoff remains stable in an $(n + 1)$ -dimensional FRW universe. For the Tsallis HDE scenario, the horizon entropy is given by

$$S_h = \gamma r_h^{2\sigma} \quad (2)$$

where γ_t is a constant in terms of the Planck area, and the Tsallis parameter is σ . Using the Tsallis entropy, one can write the holographic DE energy density as

$$\rho = \frac{3c^2}{R_h^{4-2\sigma}} \quad (3)$$

where R_h here refers the infrared cutoff scale, similar to the one in the simple holographic energy density. Furthermore, we shall consider that there is no interaction happening between the dark energy and dark matter sectors in this work. In the non-viscous scenario, the equation of state is the usual $p = w\rho$, where w is the equation of state parameter. The equation of state that we consider for the viscous fluid configuration is given by [86,87]

$$p = w\rho - 3\epsilon_0 H \quad (4)$$

where ϵ_0 is a thermodynamic parameter, which can be considered to be either time-dependent or time-independent. In this scenario, we consider dark energy to be a viscous holographic dark fluid while next, we will also be considering a generalized Chaplygin gas model [88], characterized by the EOS

$$p = -\frac{A}{\rho^\alpha} \quad (5)$$

where A and α are assumed to be positive constants, where for $\alpha = 1$, one obtains the usual Chaplygin gas model. In this scenario, we shall be considering dark energy to be a holographic Chaplygin gas. Furthermore, we shall be considering an ansatz for the scale factor of the power law form as follows [36,89–94]

$$a(t) = a_0(t_s - t)^n. \quad (6)$$

The above form of the scale factor has been used in various seminal works to understand the late time acceleration of the universe, and even cosmological singularities (see [95,96] for recent reviews on the same) by Odintsov, Nojiri, Barrow et al., and is fit to be used for our purposes too as it accounts for a lot of interesting cosmological epochs. Such an ansatz-based approach to holographic dark energy has recently been pursued in other works too [71–73,97].

3. Analysis of the Various Scenarios

3.1. Non-Viscous Fluid Case

Choosing the conventional holographic dark energy density:

$$\rho_\Lambda = \frac{3c^2}{R_h^2} \quad (7)$$

where c is a constant, and choosing the scale to correspond with the event horizon, with the R_h being the future event horizon given by:

$$R_h = a \int_t^\infty \frac{dt}{a} = a \int_a^\infty \frac{da}{Ha^2} \quad (8)$$

The critical energy density, ρ_{cr} , is given by the following relation:

$$\rho_{cr} = 3H^2 \quad (9)$$

Now, we define the dimensionless dark energy as:

$$\Omega_\Lambda = \frac{\rho_\Lambda}{\rho_{cr}} = \frac{c^2}{R_h^2 H^2} \quad (10)$$

Using the definition of Ω_Λ and the relation for \dot{R}_h from Equations (8)–(10), we have:

$$\dot{R}_h = R_h H - 1 = \frac{c}{\sqrt{\Omega_\Lambda}} - 1 \quad (11)$$

By considering the definition of holographic energy density ρ_Λ and using the expressions for Ω_Λ and \dot{R}_h , we can find:

$$\dot{\rho}_\Lambda = -2H \left(1 - \frac{\sqrt{\Omega_\Lambda}}{c} \right) \rho_\Lambda \quad (12)$$

Substituting this relation into the following equation:

$$\dot{\rho}_\Lambda + 3H(1 + w_\Lambda)\rho_\Lambda = 0 \quad (13)$$

we obtain:

$$w_\Lambda = - \left(\frac{1}{3} + \frac{2\sqrt{\Omega_\Lambda}}{3c} \right) \quad (14)$$

Instead, if we use the Tsallis holographic energy density, we can write

$$\rho_\Lambda = \frac{3c^2}{R_h^{4-2\sigma}}$$

where σ is the Tsallis parameter. Using this, we can write Ω as

$$\Omega = \frac{\rho_\Lambda}{\rho_{cr}} = \frac{3c^2}{R_h^{4-2\sigma}} \quad (15)$$

One can then write (5) as

$$\dot{R}_h = R_h H - 1 = \frac{c}{\sqrt{\Omega_\Lambda} R_h^{1-\sigma}} - 1 \quad (16)$$

Furthermore, the equation for $\dot{\rho}_\Gamma$ in this scenario takes the shape

$$\dot{\rho}_\Lambda = -(4 - 2\sigma)\rho H \left[1 - \frac{\sqrt{\Omega_\Lambda} R_h^{1-\sigma}}{c} \right] \quad (17)$$

And, finally, this leads us to the equation-of-state parameter to be

$$w_\Lambda = - \left[\frac{2\sigma - 1}{3} + \frac{(4 - 2\sigma)\sqrt{\Omega_\Lambda} R_h^{1-\sigma}}{3c} \right] \quad (18)$$

Two things to observe here is that, firstly, these equations are consistent with the usual HDE model represented by (7) as these equations reduce to that when $\sigma = 1$, as it should for any Tsallis HDE model. The second thing, which is more interesting, is that one observes that w_Λ becomes very dynamical and acquires time dependence because of the existence of the factor $R_h^{1-\sigma}$ in its expression. One can work out time-dependent expression for R_h then by considering different ansatz for both the scale factor and the Hubble parameter, see [71] where three different ansatz for the scale factor were used to study an HDE model in a Gauss–Bonnet cosmology. What is immediately clear in this regard, in the context of Tsallis cosmology, is that it provides for a far more dynamical view with regards to the phantom divide than usual HDE models, and one could cross the phantom divide even for a non interacting model, as in this case we have not assumed any interaction between dark energy and dark matter. Furthermore, the time-dependent behaviour of the w parameter for Tsallis models can have even more interesting implications for astronomical tensions like the H_0 tension, possibly.

Now, we select the scale factor to be of the form (6) (while one can certainly think about other alternative forms of the scale factor ansatz like in [71–73,97], the different scale factor choices are quite similar in the sense that they, in some way or the other, represent power law forms. Hence, even though we can perform the analysis for another choice of the scale factor, for now we will be focused on this form only here).

$$a(t) = a_0(t_s - t)^n$$

Using this, one can find the future event horizon by solving

$$\dot{R}_h = R_h H - 1 = \frac{c}{\sqrt{\Omega_\Lambda}} - 1 \quad (19)$$

to be

$$R_h(t) = \frac{C_1(n-1)(t-t_s)^n + t-t_s}{n-1} \quad (20)$$

where C_1 is some constant of integration. Now, using this, we can write (18) as

$$w = \frac{1}{3} \left(-\frac{\sqrt{\Omega}(4-2\sigma) \left(C_1(t-t_s)^n + \frac{t-t_s}{n-1} \right)^{1-\sigma}}{c} - 2\sigma + 1 \right) \quad (21)$$

Now, in order to proceed further, we need to set some values for the parameters. One good choice would be $c = 0.3, c_1 = 0.01, n = 3, \Omega = 0.69$, and $t_s = 0.002$ with $\Omega = 0.69$. Using these, we can plot the equation of the state parameter for different values of σ .

As is clear from Figure 1, one sees that, while steadily increasing σ values from over 1 to >2 , one sees a very curious behavior of the EOS of the HDE. While for $\sigma = 1.1$, the EOS mostly stays in the deep phantom regions, with no hope of ever even reaching near $w \rightarrow -1$; for a larger value of $\sigma = 1.7$, the EOS starts from the phantom regime, crosses the -1 barrier, and ascends to some degree to the quintessence region as well. For $\sigma > 2$, however, in the case where $\sigma = 2.3$, for example, the EOS shows the opposite behavior. It starts off in the deep quintessence regime, after which it crosses the -1 barrier to descend into the phantom regime to some degree. Furthermore, the expression for energy density in this scenario takes the form

$$\begin{aligned} \rho(t) = \rho_0 \exp & \left(2(\sigma - 2) \left(\frac{\sqrt{\sigma} \Gamma\left(\frac{n\sigma-1}{n-1}\right) \left(\frac{(t-t_s)^{1-n}}{c_1(n-1)} + 1\right)^\sigma (c_1(t-t_s)^n + \frac{t-t_s}{n-1})^{-\sigma}}{(n-1)^2(c-c\sigma)} \right) \right) \\ & + \left(\frac{(c_1(n-1)^2(t-t_s)^n, 2\tilde{F}1\left(\frac{n(\sigma-1)}{n-1}, \sigma, \frac{n\sigma-1}{n-1}, \frac{(t-t_s)^{1-n}}{c_1(n-1)}\right))}{(n-1)^2(c-c\sigma)} \right) \\ & + \frac{+n(\sigma-1)(t-t_s), 2\tilde{F}1\left(\sigma, \frac{n\sigma-1}{n-1}, \frac{\sigma n+n-2}{n-1}, \frac{(t-t_s)^{1-n}}{c_1(n-1)}\right)}{(n-1)^2(c-c\sigma)} - n \log(t-t_s) t_s \end{aligned} \tag{22}$$

where $2\tilde{F}1$ refers to the hypergeometric function. While the expression above looks quite humongous, which it indeed is, we can plot it for a similar choice of parameters as we did previously.

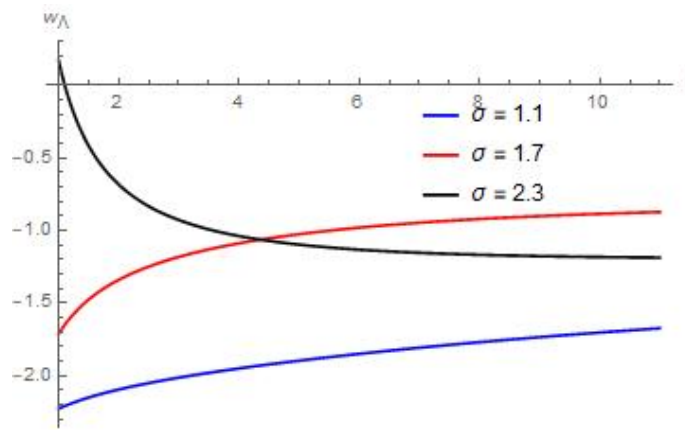


Figure 1. A plot of the dark energy EOS with time, plotted for increasing σ values.

One sees from Figure 2 that, for progressively increasing values of σ , the variation of the energy density with respect to time becomes smaller and smaller, as for $\sigma = 1.3$ and $\sigma = 1.5$, one sees that the energy density fluctuates a lot, while for higher values of $\sigma = 1.9$ and $\sigma = 2.2$, it almost takes the shape of a constant curve.

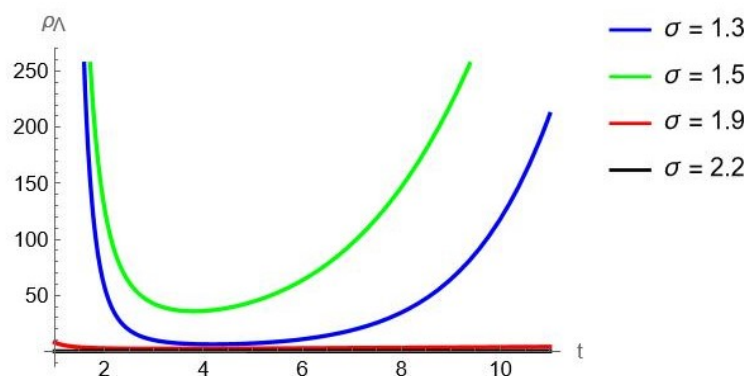


Figure 2. A plot of the DE energy density ρ_Λ with time, plotted for increasing σ values.

This brings us to another interesting issue with the usual HDE models, which the Tsallis model with event horizon cutoff can possibly handle optimistically, in the way that we have dealt with it here. This concerns the issue of classical instabilities of perturbations in HDE models, which was first shown in [98]. The key for this lies in the squared speed of sound, which for our case would take the form

$$v_s^2 = \frac{\dot{p}}{\dot{\rho}} \tag{23}$$

The sign of v_s^2 is crucial for determining the stability of background evolution, with negative v_s^2 for a model highlighting that the model has classical instabilities for any given perturbation. In [98], it was shown that conventional HDE models would have this instability and, recently, a paper also showed that Tsallis HDE can bypass this issue in interacting scenarios [99,100], but nobody has considered whether these issues can be bypassed in a non interacting scenario, so here we can actually show that the same can happen for a non interacting scenario as well. The squared sound speed for our model can be written as

$$v_{sv}^2 = \frac{1}{3} \left(\frac{\sqrt{\Omega}(\sigma - 1)R_h(t)R'_h(t)}{h(t)(cR_h(t)^\sigma - \sqrt{\Omega}R_h(t))} + \frac{2\sqrt{\Omega}(\sigma - 2)R_h(t)^{1-\sigma}}{c} - 2\sigma + 1 \right) \tag{24}$$

Plugging in the expression for $R_h(t)$ from before, we get

$$v_{sv}^2 = \frac{1}{3} \left(- \frac{\sqrt{\Omega}(1-\sigma)(c_1(n-1)n(t-t_s)^{n-1}+1)(c_1(t-t_s)^n + \frac{t-t_s}{n-1})^{1-\sigma}}{(n-1)h(t) \left(c - \sqrt{\Omega} \left(c_1(t-t_s)^n + \frac{t-t_s}{n-1} \right)^{1-\sigma} \right)} - \frac{\sqrt{\Omega}(4-2\sigma)(c_1(t-t_s)^n + \frac{t-t_s}{n-1})^{1-\sigma}}{c} - 2\sigma + 1 \right) \tag{25}$$

One can clearly see from Figure 3 that one can get rid of the stability issues persistent in normal HDE models in a Tsallis HDE scenario. Particularly, one sees that, for very small values of σ , in this $\sigma = 0.6$ (which is even lower than the σ for recovering simple HDE), there is no hope of escaping the instability issues, as v_s^2 is always negative. However, as one increases the values of σ and one gradually starts to deviate away from the usual HDE models, there is a gradual departure from the instability problem v_s^2 for all of $\sigma = (1.5, 1.9, 2.2)$, which obtains positive values even though they could initially have negative values. This shows that Tsallis models with higher values of the Tsallis parameters offer classical stability and, as one deviates away from the usual HDE scenario, one obtains models which have more and more classical stability in the face of perturbations. But even the higher values of σ eventually tend to instability as time progresses. It is helpful to see the behavior of the squared sound speed values at arbitrarily large values.

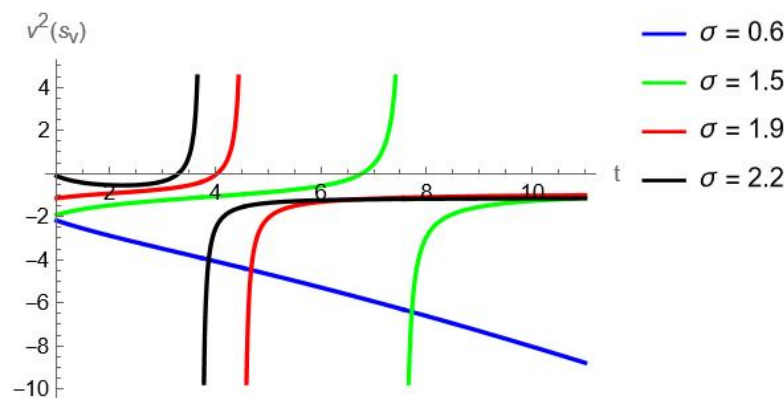


Figure 3. A plot of the squared sound speed v_s^2 for the event horizon cutoff Tsallis model with time, plotted for increasing σ values.

One sees from Figure 4 that, far ahead in time, the models corresponding to all these various values of σ eventually acquire classical instability as they have negative squared sound speeds.

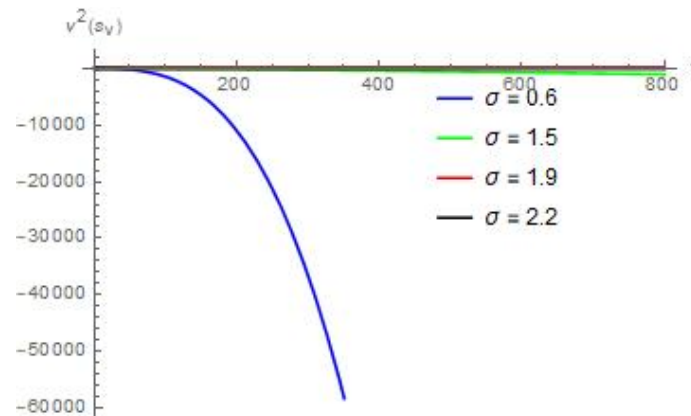


Figure 4. A plot of the squared sound speed v_s^2 for the event horizon cutoff viscous Tsallis model with time, plotted for increasing σ values in an arbitrarily large timeframe.

3.2. Viscous Fluid Case

While we are already obtaining very interesting results for the Tsallis model for conventional fluids with $p = w\rho$, one can go beyond this too. Particularly, let us consider the case of viscous and Chaplygin gas fluids. The equation-of-state that we consider for the viscous fluid configuration is given by [86,87]

$$p = w\rho - 3\epsilon_0 H \quad (26)$$

where ϵ_0 is a thermodynamic parameter which can be considered to be either time-dependent or time-independent. As we shall see, this parameter does not directly impact any of our calculations. Using (7), we can write the continuity equation in this case to be

$$-(4 - 2\sigma)\rho H \left[1 - \frac{\sqrt{\Omega_\Lambda} R_h^{1-\sigma}}{c} \right] + 3H(\rho(1 + w_v) - 3\epsilon_0 H) = 0 \quad (27)$$

where w_v is the EOS for HDE in the case of the viscous fluid configuration. Working with the above equation, after some effort, one can reach for w to be

$$w_v = w_v = -\frac{1}{3}(4 - 2\sigma) \left(1 - \frac{\sqrt{\Omega_\Lambda} R_h(t)^{1-\sigma}}{c} \right) - 1 \quad (28)$$

Using the expression for $R_h(t)$, one can then write

$$w_v = -\frac{1}{3}(4 - 2\sigma) \left(1 - \frac{\sqrt{\Omega_\Lambda} \left(c_1(t - t_s)^n + \frac{t-t_s}{n-1} \right)^{1-\sigma}}{c} \right) - 1 \quad (29)$$

As one sees from Figure 5, the dark energy EOS again crosses the phantom divide but the behavior here is completely the opposite to what one observes for the non-viscous fluid case in Figure 1. Particularly, one sees that, for smaller values of σ , like $\sigma = 1.1$ in this case, which represents possibly the smallest deviation from the normal HDE to the Tsallis model, the EOS starts off in the deep quintessence region and never really hits the $w = -1$ region, let alone crossing the phantom barrier. While the higher values of σ in this case like $\sigma = (1.5, 1.8)$ start off in the quintessence region and descend to phantom while the very high values, like $\sigma = 2.2$, start from the deep phantom region and only go over ever so slightly above -1 into a very small patch of the quintessence regime. The phantom divide happens again but in a completely opposite fashion to the trend seen in the non-viscous fluid case. The energy density of dark energy fluctuates in pretty much the same way as in

Figure 2, the same for the non-viscous regime as in the viscous regime and so we do not need to show its plot here.

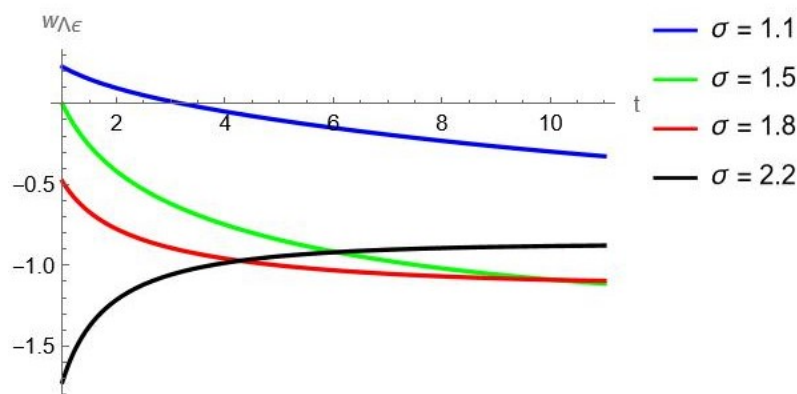


Figure 5. A plot of the dark energy EOS for the event horizon cutoff Tsallis model with viscous fluid configuration w_v with time, plotted for increasing σ values.

The sound speed squared in this case turns out to be

$$v_{sv}^2 = \frac{1}{3} \left(\sqrt{\Omega} \left(\frac{(\sigma - 1)R_h \dot{h}(t)}{h(t) (\sqrt{\Omega}R_h(t) - cR_h(t)^\sigma)} + \frac{2(\sigma - 2)R_h(t)^{1-\sigma}}{c} \right) - 2\sigma + 1 \right) \quad (30)$$

which, using the expression we have for the future event horizon, becomes

$$v_{sv}^2 = \frac{1}{3} (4 - 2\sigma) \left(- \frac{\sqrt{\Omega} (c_1(t-t_s)^n + \frac{t-t_s}{n-1})^{1-\sigma}}{c} + \frac{\sqrt{\Omega}(\sigma-1)(c_1(n-1)n(t-t_s)^n + t-t_s)}{2(\sigma-2) (n\sqrt{\Omega}(c_1(n-1)(t-t_s)^n + t-t_s) - c(n-1)n(c_1(t-t_s)^n + \frac{t-t_s}{n-1})^\sigma)} + 1 \right) - 1 \quad (31)$$

One clearly sees that there is a similarity to the trend in the graphs of the squared sound speed in both the viscous and non-viscous cases as given by Figures 3 and 6, respectively. We again see that, for very small values of σ , there is no hope to avoid classical instabilities even in the viscous Tsallis model, while one can hope for better results as one increases the value of σ . Hence, one sees that, as one increases the deviation from the usual HDE model, and with the effects of the Tsallis model becoming more and more apparent, the stability of the model has a hope of becoming stable. But again, even the higher values of σ eventually tend to instability. In this scenario, it is especially helpful to see the behavior at arbitrarily large times.

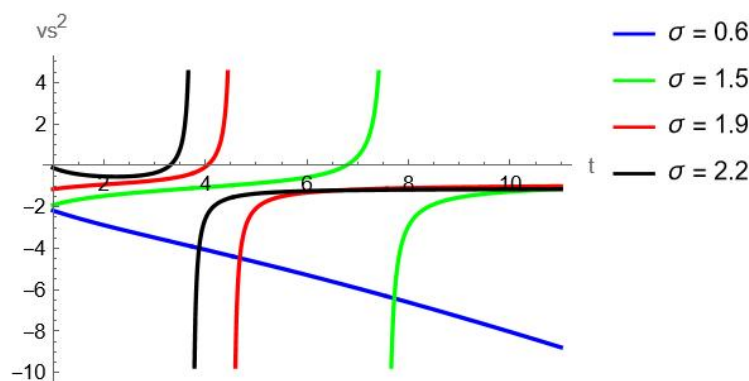


Figure 6. A plot of the squared sound speed v_s^2 for the event horizon cutoff viscous Tsallis model with time, plotted for increasing σ values.

As is clear from Figure 7, as time progresses to very large values, models for all values of σ eventually attain negative squared sound speed values. Hence, all these models likely become unstable for perturbations in large timeframes.

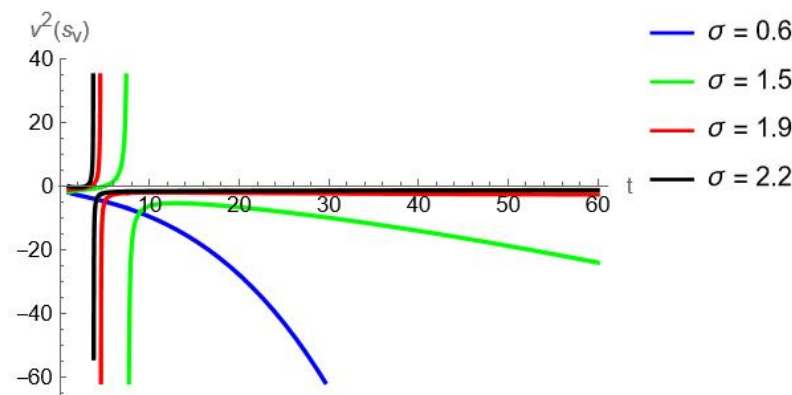


Figure 7. A plot of the squared sound speed v_s^2 for the event horizon cutoff viscous Tsallis model with time, plotted for increasing σ values at arbitrarily large times.

3.3. Chaplygin Gas Case

Until now, both the models that we have discussed have given interesting results from the perspective of the phantom divide, showing that the Tsallis model can show such a divide for a nice range of the Tsallis parameter for both viscous and non viscous fluid configurations. But although in these paradigms we are seeing small hints of escaping the issues of classical instability, as pointed out in [98], the instability eventually takes over in these models as time progresses. Now, we turn our attention to the generalized Chaplygin gas model, characterized by the EOS

$$p = -\frac{A}{\rho^\alpha} \quad (32)$$

where A and α are assumed to be positive constants, where for $\alpha = 1$, one obtains the usual Chaplygin gas model. Now, for a Tsallis HDE scenario with a Chaplygin gas configuration, we can write the continuity equation to be

$$-(4 - 2\sigma)\rho H \left[1 - \frac{\sqrt{\Omega_\Lambda} R_h^{1-\sigma}}{c} \right] + 3H \left(\rho - \frac{A}{\rho^\alpha} \right) = 0 \quad (33)$$

from which we can write the EOS to be

$$w_c = +\frac{1}{3}(4 - 2\sigma) \left(1 - \frac{\sqrt{\Omega_\Lambda} R_h(t)^{1-\sigma}}{c} \right) - 1 \quad (34)$$

Using the expression for the future event horizon, we can write

$$w_c = \frac{1}{3}(4 - 2\sigma) \left(1 - \frac{\sqrt{\bar{o}} \left(c_1(t - t_s)^n + \frac{t - t_s}{n-1} \right)^{1-\sigma}}{c} \right) - 1 \quad (35)$$

As one can see from Figure 8, for relatively smaller values of time, the larger values of σ (in this case $\sigma = (1.5, 1.9, 2.2)$) cross the -1 barrier starting either from the quintessence or phantom regime while the smallest value of σ , which in this case is $\sigma = 1.1$, appears to not be able to do so in this timeframe. Plotting for arbitrarily large times, however, gives us the following plot.

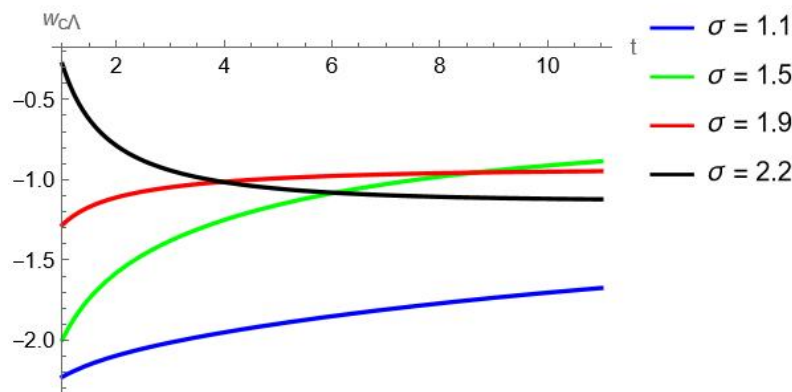


Figure 8. A plot of the dark energy EOS for the event horizon cutoff Tsallis model with Chaplygin gas configuration w_c with time, plotted for increasing σ values.

For large values of time, or equivalently speaking, as time progresses further and further, one sees from Figure 9 that even the model with the slightest deviation from the simple HDE, $\sigma = 1.1$, also crosses the -1 barrier and eventually ascends into the quintessence regime. While the model for $\sigma = 1.5$ becomes well settled in the quintessence regime, with $\sigma = (1.9, 2.2)$ models becoming settled in the phantom regime. The thing to note, very interestingly, is that the Chaplygin gas parameters, A and α , do not impact the behavior of the equation-of-state at all and do not factor into the equation in any case. One can also consider the energy density of the HDE in this case, which can be written as

$$\rho_{\Lambda c} = 3^{\frac{1}{\alpha+1}} \left(\frac{acR_h(t)^\sigma}{c(2\sigma - 1)R_h(t)^\sigma - 2\sqrt{\Omega}(\sigma - 2)R_h(t)} \right)^{\frac{1}{\alpha+1}} \tag{36}$$

Plotting the expression of the future event horizon, we get

$$\rho_{\Lambda c} = 3^{\frac{1}{\alpha+1}} \left(\frac{a}{3 - (4 - 2\sigma) \left(1 - \frac{\sqrt{\Omega}(c_1(t-t_s)^n + \frac{t-t_s}{n-1})^{1-\sigma}}{c} \right)} \right)^{\frac{1}{\alpha+1}} \tag{37}$$

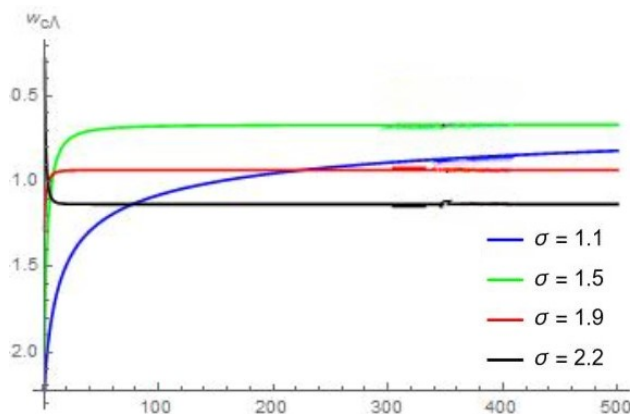


Figure 9. A plot of the dark energy EOS for the event horizon cutoff Tsallis model with Chaplygin gas configuration w_c with time, plotted for increasing σ values, plotted for a large timeframe.

As one sees from Figure 10, the density fluctuates in different ways for all values of σ , but the trends of the evolution of the densities stays quite the same for different values of A . Plotting for one of these values at large times, say $A = 2$, we have

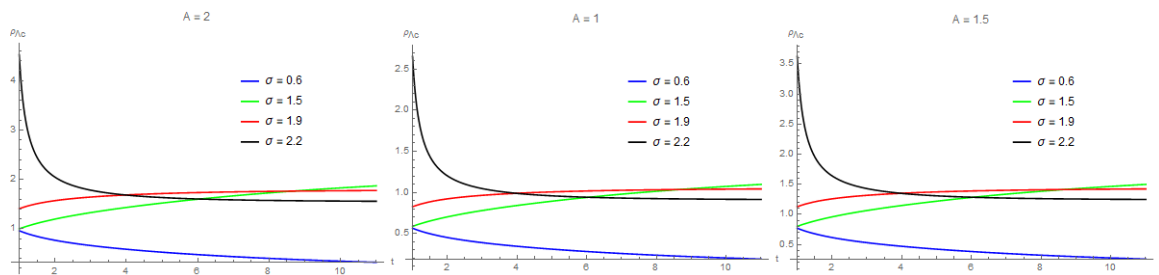


Figure 10. A plot of the DE energy density $\rho_{\Lambda c}$, plotted for increasing σ values and plotted for different values of A against time.

We see from Figure 11 that, eventually, it is not the value which is not too high, like $\sigma = 2.2$, or not too low, like $\sigma = 1.1$ m, but rather the intermediate value, which is $\sigma = 1.5$, which eventually has the highest values of the energy density of the HDE. The evolution of all the densities in different models is again different but is pretty much a smooth transition from what is observed for smaller timeframes in Figure 10.

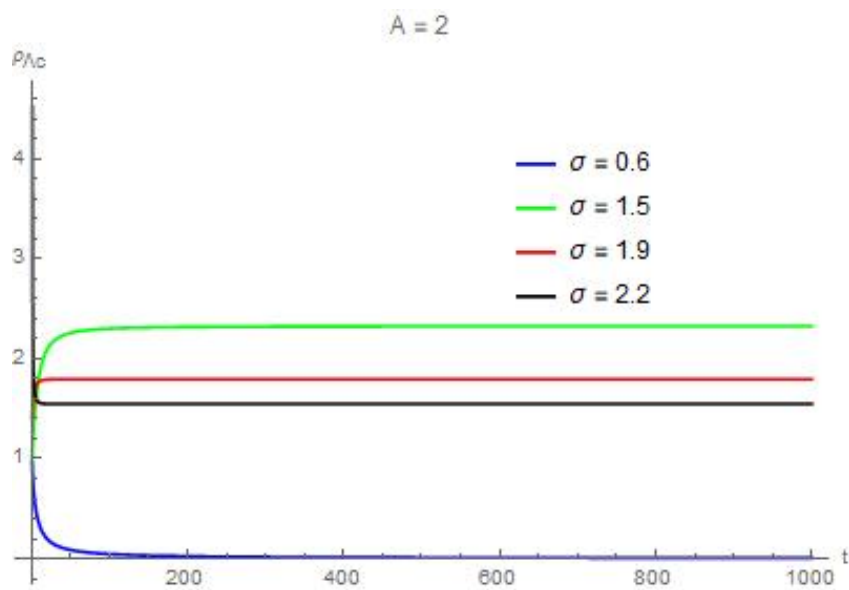


Figure 11. A plot of the DE energy density $\rho_{\Lambda c}$, plotted for increasing σ values plotted for different values of A against time.

Now, we finally turn our attention to what is perhaps the most surprising discovery here. The squared speed in the case of the Chaplygin gas scenario can be written as

$$v_{sc}^2 = \frac{1}{3}\alpha \left(3 - (4 - 2\sigma) \left(1 - \frac{\sqrt{\Omega} R_h(t)^{1-\sigma}}{c} \right) \right) \tag{38}$$

And again, by using the expression of the future event horizon, we can write

$$v_{sc}^2 = \alpha - \frac{1}{3}\alpha(4 - 2\sigma) \left(1 - \frac{\sqrt{\Omega} \left(c_1(t - t_s)^n + \frac{t-t_s}{n-1} \right)^{1-\sigma}}{c} \right) \tag{39}$$

Plotting this against time, in Figure 12, we plot the sound speed squared for different values of σ setting $\alpha = 0.3$ (the trend of the sound speed stays the same for $\alpha \leq 1$).

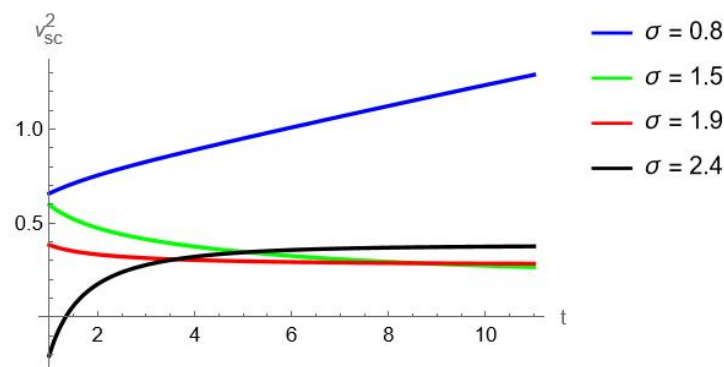


Figure 12. A plot of the squared sound speed v_{sc}^2 , plotted for increasing σ values plotted for $\alpha = 0.3$ against time.

The plot shown in Figure 12 is quite interesting. One sees that, for all values of σ in this case, which are $\sigma = (0.8, 1.5, 1.9, 2.4)$, there is a clear and very evident preference of the squared sound speed towards highly positive values. In fact, only the highest value of σ in this case, which is $\sigma = 2.4$, picks up negative values of the squared sound speed in the very beginning while it very quickly ascends to positive values. In a larger timeframe, the plot takes the shape.

One sees from Figure 13 that, in arbitrarily large time frames or, equivalently speaking, as time progresses further and further on, various σ models very easily and definitively maintain classical stability as they eventually have quite substantial positive values for the squared sound speed. This definitively stable behavior from the perturbations point of view is seen very convincingly in the case of the Tsallis Chaplygin gas scenario, something which we only saw in very small patches for the previous two Tsallis models that we considered.

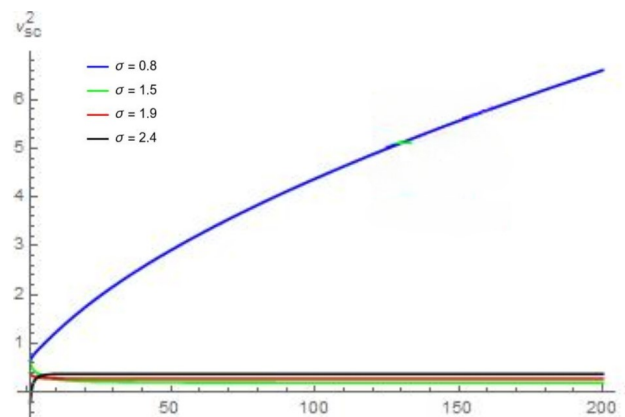


Figure 13. A plot of the squared sound speed v_{sc}^2 , plotted for increasing σ values plotted for $\alpha = 0.3$ against time.

4. Conclusions

In this work, we considered the Tsallis holographic dark energy model in a scale factor ansatz-based approach. Holographic dark energy models have gained considerable interest in recent times as a quantum gravity-motivated explanation of dark energy and, while it shows promising features quite often, it has its own set of issues. One of the primary issues which often plagues these models is the issue of classical instability, characterized by superluminal or negative squared sound speeds. Another issue is the unrealistic evolution of the dark energy EOS parameter, and so in this work, we consider the status quo of simple power law models in a Tsallis HDE scenario with no interacting dark sector. What

motivated such a study is the fact that it becomes very hard to have a consistent HDE scenario both when one considers non-interacting dark sectors and also when one considers simple power law models, and so this work went on to see to what extent one would have to churn up this HDE model in order to end up with a consistent paradigm. We considered the event horizon cutoff for our analysis while considering three different cosmological settings for our model, namely with non-viscous, viscous, and Chaplygin gas configurations. We were able to show that, in all such cases, one can clearly see that the Tsallis models cross the phantom divide but stability issues persist throughout the reasonable range of the Tsallis parameters in both viscous and non-viscous cases. But, interestingly, the Chaplygin gas models present us with more stable dark energy scenarios as they give long term stability. This points towards the notion that HDE scenarios, when also supplemented with non-trivial EOS forms for DE (like the Chaplygin or the generalized Chaplygin in our case), can perhaps provide consistent scenarios even in those regimes where it is otherwise too difficult for HDEs to provide stable paradigms.

Author Contributions: Conceptualization, O.T.; methodology, O.T.; validation, O.T., M.K. and A.V.T.; formal analysis, O.T.; investigation, O.T., M.K. and A.V.T.; writing—original draft preparation, O.T.; writing—review and editing, M.K. and A.V.T.; visualization, O.T.; supervision, M.K. and A.V.T.; project administration, O.T., M.K. and A.V.T.; funding acquisition, M.K. and A.V.T. All authors have read and agreed to the published version of the manuscript.

Funding: The research by M.K. was carried out at Southern Federal University with financial support from the Ministry of Science and Higher Education of the Russian Federation (State contract GZ0110/23-10-IF). The work of A.T. was supported by Russian Foundation for Basic Research; Project No. 20-52-05009.

Data Availability Statement: No new data are associated with this work.

Conflicts of Interest: The authors declare no conflicts of interest.

References

1. Riess, A.G.; Filippenko, A.V.; Challis, P.; Clocchiatti, A.; Diercks, A.; Garnavich, P.M.; Gilliland, R.L.; Hogan, C.J.; Jha, S.; Kirshner, R.P. Observational evidence from supernovae for an accelerating universe and a cosmological constant. *Astron. J.* **1998**, *116*, 1009–1038. [[CrossRef](#)]
2. Weinberg, S. The Cosmological Constant Problem. *Rev. Mod. Phys.* **1989**, *61*, 1–23. [[CrossRef](#)]
3. Lombriser, L. On the cosmological constant problem. *Phys. Lett. B* **2019**, *797*, 134804. [[CrossRef](#)]
4. Padmanabhan, T. Cosmological constant: The Weight of the vacuum. *Phys. Rep.* **2003**, *380*, 235–320. [[CrossRef](#)]
5. Capozziello, S.; De Laurentis, M. Extended Theories of Gravity. *Phys. Rep.* **2011**, *509*, 167–321. [[CrossRef](#)]
6. Nojiri, S.; Odintsov, S.D. Unified cosmic history in modified gravity: From F(R) theory to Lorentz non-invariant models. *Phys. Rep.* **2011**, *505*, 59–144. [[CrossRef](#)]
7. Nojiri, S.; Odintsov, S.D.; Oikonomou, V.K. Modified Gravity Theories on a Nutshell: Inflation, Bounce and Late-time Evolution. *Phys. Rep.* **2017**, *692*, 1–104. [[CrossRef](#)]
8. Zlatev, I.; Wang, L.M.; Steinhardt, P.J. Quintessence, cosmic coincidence, and the cosmological constant. *Phys. Rev. Lett.* **1999**, *82*, 896–899. [[CrossRef](#)]
9. Tsujikawa, S. Quintessence: A Review. *Class. Quant. Grav.* **2013**, *30*, 214003. [[CrossRef](#)]
10. Faraoni, V. Inflation and quintessence with nonminimal coupling. *Phys. Rev. D* **2000**, *62*, 023504. [[CrossRef](#)]
11. Gasperini, M.; Piazza, F.; Veneziano, G. Quintessence as a runaway dilaton. *Phys. Rev. D* **2002**, *65*, 023508. [[CrossRef](#)]
12. Capozziello, S.; Carloni, S.; Troisi, A. Quintessence without scalar fields. *Recent Res. Dev. Astron. Astrophys.* **2003**, *1*, 625.
13. Capozziello, S. Curvature quintessence. *Int. J. Mod. Phys. D* **2002**, *11*, 483–492. [[CrossRef](#)]
14. Odintsov, S.D.; Oikonomou, V.K.; Giannakoudi, I.; Fronimos, F.P.; Lymperiadou, E.C. Recent Advances on Inflation. *Symmetry* **2023**, *15*, 9. [[CrossRef](#)]
15. Sahni, V.; Shtanov, Y. Brane world models of dark energy. *J. Cosmol. Astropart. Phys.* **2003**, *11*, 014. [[CrossRef](#)]
16. Sami, M.; Sahni, V. Quintessential inflation on the brane and the relic gravity wave background. *Phys. Rev. D* **2004**, *70*, 083513. [[CrossRef](#)]
17. Tretyakov, P.; Toporensky, A.; Shtanov, Y.; Sahni, V. Quantum effects, soft singularities and the fate of the universe in a braneworld cosmology. *Class. Quant. Grav.* **2006**, *23*, 3259–3274. [[CrossRef](#)]
18. Chen, S.; Wang, B.; Jing, J. Dynamics of interacting dark energy model in Einstein and Loop Quantum Cosmology. *Phys. Rev. D* **2008**, *78*, 123503. [[CrossRef](#)]

19. Fu, X.; Yu, H.W.; Wu, P. Dynamics of interacting phantom scalar field dark energy in Loop Quantum Cosmology. *Phys. Rev. D* **2008**, *78*, 063001. [[CrossRef](#)]
20. Bonanno, A.; Reuter, M. Cosmology with selfadjusting vacuum energy density from a renormalization group fixed point. *Phys. Lett. B* **2002**, *527*, 9–17. [[CrossRef](#)]
21. Bonanno, A.; Reuter, M. Cosmology of the Planck era from a renormalization group for quantum gravity. *Phys. Rev. D* **2002**, *65*, 043508. [[CrossRef](#)]
22. Bentivegna, E.; Bonanno, A.; Reuter, M. Confronting the IR fixed point cosmology with high redshift supernova data. *J. Cosmol. Astropart. Phys.* **2004**, *2004*, 001. [[CrossRef](#)]
23. Reuter, M.; Saueressig, F. From big bang to asymptotic de Sitter: Complete cosmologies in a quantum gravity framework. *J. Cosmol. Astropart. Phys.* **2005**, *2005*, 012. [[CrossRef](#)]
24. Bonanno, A.; Reuter, M. Entropy signature of the running cosmological constant. *J. Cosmol. Astropart. Phys.* **2007**, *2007*, 024. [[CrossRef](#)]
25. Weinberg, S. Asymptotically Safe Inflation. *Phys. Rev. D* **2010**, *81*, 083535. [[CrossRef](#)]
26. Trivedi, O.; Khlopov, M. Singularity formation in asymptotically safe cosmology with inhomogeneous equation of state. *J. Cosmol. Astropart. Phys.* **2022**, *2022*, 007. [[CrossRef](#)]
27. Trivedi, O.; Khlopov, M. On finite time singularities in scalar field dark energy models based in the RS-II Braneworld. *Eur. Phys. J. C* **2022**, *82*, 800. [[CrossRef](#)]
28. Aghanim, N.; Akrami, Y.; Ashdown, M.; Aumont, J.; Baccigalupi, C.; Ballardini, M.; Banday, A.J.; Barreiro, R.B.; Bartolo, N.; Basak, S.; Battye, R. Planck 2018 results. VI. Cosmological parameters. *Astron. Astrophys.* **2020**, *641*, A6; Erratum in *Astron. Astrophys.* **2021**, *652*, C4. [[CrossRef](#)]
29. Riess, A.G.; Casertano, S.; Yuan, W.; Macri, L.M.; Scolnic, D. Large Magellanic Cloud Cepheid standards provide a 1% foundation for the determination of the Hubble constant and stronger evidence for physics beyond Λ CDM. *Astrophys. J.* **2019**, *876*, 85. [[CrossRef](#)]
30. Riess, A.G.; Yuan, W.; Macri, L.M.; Scolnic, D.; Brout, D.; Casertano, S.; Jones, D.O.; Murakami, Y.; Breuval, L.; Brink, T.G.; et al. A Comprehensive Measurement of the Local Value of the Hubble Constant with 1 km/s/Mpc Uncertainty from the Hubble Space Telescope and the SH0ES Team. *arXiv* **2021**, arXiv:2112.04510.
31. 't Hooft, G. Dimensional reduction in quantum gravity. *Conf. Proc. C* **1993**, *930308*, 284–296.
32. Susskind, L. The World as a hologram. *J. Math. Phys.* **1995**, *36*, 6377–6396. [[CrossRef](#)]
33. Bousso, R. A Covariant entropy conjecture. *JHEP* **1999**, *1999*, 004. [[CrossRef](#)]
34. Cohen, A.G.; Kaplan, D.B.; Nelson, A.E. Effective field theory, black holes, and the cosmological constant. *Phys. Rev. Lett.* **1999**, *82*, 4971–4974. [[CrossRef](#)]
35. Wang, S.; Wang, Y.; Li, M. Holographic Dark Energy. *Phys. Rep.* **2017**, *696*, 1–57. [[CrossRef](#)]
36. Nojiri, S.; Odintsov, S.D. Unifying phantom inflation with late-time acceleration: Scalar phantom-non-phantom transition model and generalized holographic dark energy. *Gen. Rel. Grav.* **2006**, *38*, 1285–1304. [[CrossRef](#)]
37. Nojiri, S.; Odintsov, S.D. Covariant Generalized Holographic Dark Energy and Accelerating Universe. *Eur. Phys. J. C* **2017**, *77*, 528. [[CrossRef](#)]
38. Nojiri, S.; Odintsov, S.D.; Paul, T. Different Faces of Generalized Holographic Dark Energy. *Symmetry* **2021**, *13*, 928. [[CrossRef](#)]
39. Nojiri, S.; Odintsov, S.D.; Oikonomou, V.K.; Paul, T. Unifying Holographic Inflation with Holographic Dark Energy: A Covariant Approach. *Phys. Rev. D* **2020**, *102*, 023540. [[CrossRef](#)]
40. Oliveros, A.; Sabogal, M.A.; Acero, M.A. Barrow holographic dark energy with Granda–Oliveros cutoff. *Eur. Phys. J. Plus* **2022**, *137*, 783. [[CrossRef](#)]
41. Granda, L.N.; Oliveros, A. Infrared cut-off proposal for the Holographic density. *Phys. Lett. B* **2008**, *669*, 275–277. [[CrossRef](#)]
42. Khurshudyan, M. Viscous holographic dark energy universe with Nojiri–Odintsov cut-off. *Astrophys. Space Sci.* **2016**, *361*, 392. [[CrossRef](#)]
43. Khurshudyan, M. On a holographic dark energy model with a Nojiri–Odintsov cut-off in general relativity. *Astrophys. Space Sci.* **2016**, *361*, 232. [[CrossRef](#)]
44. Belkacemi, M.H.; Bouhmadi-Lopez, M.; Errahmani, A.; Ouali, T. The holographic induced gravity model with a Ricci dark energy: smoothing the little rip and big rip through Gauss-Bonnet effects? *Phys. Rev. D* **2012**, *85*, 083503. [[CrossRef](#)]
45. Zhang, L.; Wu, P.; Yu, H. Unifying dark energy and dark matter with the modified Ricci model. *Eur. Phys. J. C* **2011**, *71*, 1588. [[CrossRef](#)]
46. Setare, M.R.; Jamil, M. Statefinder diagnostic and stability of modified gravity consistent with holographic and new agegraphic dark energy. *Gen. Rel. Grav.* **2011**, *43*, 293–303. [[CrossRef](#)]
47. Nozari, K.; Rashidi, N. Holographic Dark Energy from a Modified GBIG Scenario. *Int. J. Mod. Phys. D* **2010**, *19*, 219–231. [[CrossRef](#)]
48. Sheykhi, A. Interacting holographic dark energy in Brans-Dicke theory. *Phys. Lett. B* **2009**, *681*, 205–209. [[CrossRef](#)]
49. Xu, L.; Lu, J.; Li, W. Generalized Holographic and Ricci Dark Energy Models. *Eur. Phys. J. C* **2009**, *64*, 89–95. [[CrossRef](#)]
50. Wei, H. Modified Holographic Dark Energy. *Nucl. Phys. B* **2009**, *819*, 210–224. [[CrossRef](#)]
51. Setare, M.R.; Saridakis, E.N. Correspondence between Holographic and Gauss-Bonnet dark energy models. *Phys. Lett. B* **2008**, *670*, 1–4. [[CrossRef](#)]

52. Saridakis, E.N. Holographic Dark Energy in Braneworld Models with a Gauss-Bonnet Term in the Bulk. Interacting Behavior and the $w = -1$ Crossing. *Phys. Lett. B* **2008**, *661*, 335–341. [[CrossRef](#)]
53. Setare, M.R. The Holographic dark energy in non-flat Brans-Dicke cosmology. *Phys. Lett. B* **2007**, *644*, 99–103. [[CrossRef](#)]
54. Felegary, F.; Darabi, F.; Setare, M.R. Interacting holographic dark energy model in Brans–Dicke cosmology and coincidence problem. *Int. J. Mod. Phys. D* **2017**, *27*, 1850017. [[CrossRef](#)]
55. Dheepika, M.; Mathew, T.K. Tsallis holographic dark energy reconsidered. *Eur. Phys. J. C* **2022**, *82*, 399. [[CrossRef](#)]
56. Brevik, I.; Timoshkin, A.V. Holographic representation of the unified early and late universe via a viscous dark fluid. *Int. J. Geom. Meth. Mod. Phys.* **2022**, *19*, 2250113. [[CrossRef](#)]
57. Brevik, I.; Timoshkin, A.V. Holographic description of the dissipative unified dark fluid model with axion field. *Int. J. Mod. Phys. D* **2023**, *32*, 2350085. [[CrossRef](#)]
58. Nojiri, S.; Odintsov, S.D.; Faraoni, V. From nonextensive statistics and black hole entropy to the holographic dark universe. *Phys. Rev. D* **2022**, *105*, 044042. [[CrossRef](#)]
59. Nojiri, S.; Odintsov, S.D.; Saridakis, E.N. Modified cosmology from extended entropy with varying exponent. *Eur. Phys. J. C* **2019**, *79*, 242. [[CrossRef](#)]
60. Nojiri, S.; Odintsov, S.D.; Paul, T. Early and late universe holographic cosmology from a new generalized entropy. *Phys. Lett. B* **2022**, *831*, 137189. [[CrossRef](#)]
61. Nojiri, S.; Odintsov, S.D.; Paul, T. Holographic realization of constant roll inflation and dark energy: An unified scenario. *Phys. Lett. B* **2023**, *841*, 137926. [[CrossRef](#)]
62. Odintsov, S.D.; D’Onofrio, S.; Paul, T. Holographic realization from inflation to reheating in generalized entropic cosmology. *Phys. Dark Univ.* **2023**, *42*, 101277. [[CrossRef](#)]
63. D’Agostino, R. Holographic dark energy from nonadditive entropy: cosmological perturbations and observational constraints. *Phys. Rev. D* **2019**, *99*, 103524. [[CrossRef](#)]
64. Adil, S.A.; Gangopadhyay, M.R.; Sami, M.; Sharma, M.K. Late-time acceleration due to a generic modification of gravity and the Hubble tension. *Phys. Rev. D* **2021**, *104*, 103534. [[CrossRef](#)]
65. Gangopadhyay, M.R.; Sami, M.; Sharma, M.K. Phantom dark energy as a natural selection of evolutionary processes a genetic algorithm and cosmological tensions. *Phys. Rev. D* **2023**, *108*, 103526. [[CrossRef](#)]
66. Wang, D.; Koussour, M.; Malik, A.; Myrzakulov, N.; Mustafa, G. Observational constraints on a logarithmic scalar field dark energy model and black hole mass evolution in the Universe. *Eur. Phys. J. C* **2023**, *83*, 670. [[CrossRef](#)]
67. Shamir, M.F.; Meer, E. Study of compact stars in $\mathcal{R} + \alpha A$ gravity. *Eur. Phys. J. C* **2023**, *83*, 49. [[CrossRef](#)]
68. Farasat Shamir, M.; Rashid, A. Bardeen compact stars in modified $f(R)$ gravity with conformal motion. *Int. J. Geom. Meth. Mod. Phys.* **2023**, *20*, 2350026. [[CrossRef](#)]
69. Malik, A.; Shamir, M.F. Dynamics of some cosmological solutions in modified $f(R)$ gravity. *New Astron.* **2021**, *82*, 101460. [[CrossRef](#)]
70. Usman, A.; Shamir, M.F. Collapsing stellar structures in $f(R)$ gravity using Karmarkar condition. *New Astron.* **2022**, *91*, 101691. [[CrossRef](#)]
71. Pasqua, A.; Chattopadhyay, S.; Khurshudyan, M.; Aly, A.A. Behavior of Holographic Ricci Dark Energy in Scalar Gauss-Bonnet Gravity for Different Choices of the Scale Factor. *Int. J. Theor. Phys.* **2014**, *53*, 2988–3013. [[CrossRef](#)]
72. Chattopadhyay, S.; Pasqua, A. Holographic DBI-Essence Dark Energy via Power-Law Solution of the Scale Factor. *Int. J. Theor. Phys.* **2013**, *52*, 3945–3952. [[CrossRef](#)]
73. Chattopadhyay, S.; Pasqua, A.; Khurshudyan, M. New holographic reconstruction of scalar field dark energy models in the framework of chameleon Brans-Dicke cosmology. *Eur. Phys. J. C* **2014**, *74*, 3080. [[CrossRef](#)]
74. Jawad, A.; Azhar, N.; Rani, S. Entropy corrected holographic dark energy models in modified gravity. *Int. J. Mod. Phys. D* **2016**, *26*, 1750040. [[CrossRef](#)]
75. Barrow, J.D. The Area of a Rough Black Hole. *Phys. Lett. B* **2020**, *808*, 135643. [[CrossRef](#)] [[PubMed](#)]
76. Sheikhahmadi, H. On the origin of the holographic universe. *Mod. Phys. Lett. A* **2022**, *37*, 2250231. [[CrossRef](#)]
77. Tsallis, C.; Cirto, L.J.L. Black hole thermodynamical entropy. *Eur. Phys. J. C* **2013**, *73*, 2487. [[CrossRef](#)]
78. Barboza, E.M., Jr.; Nunes, R.D.C.; Abreu, E.M.C.; Ananias Neto, J. Dark energy models through nonextensive Tsallis’ statistics. *Physica A* **2015**, *436*, 301–310. [[CrossRef](#)]
79. Nunes, R.C.; Barboza, E.M., Jr.; Abreu, E.M.C.; Neto, J.A. Probing the cosmological viability of non-gaussian statistics. *J. Cosmol. Astropart. Phys.* **2016**, *2016*, 051. [[CrossRef](#)]
80. Moradpour, H. Implications, consequences and interpretations of generalized entropy in the cosmological setups. *Int. J. Theor. Phys.* **2016**, *55*, 4176–4184. [[CrossRef](#)]
81. Tavayef, M.; Sheykhi, A.; Bamba, K.; Moradpour, H. Tsallis Holographic Dark Energy. *Phys. Lett. B* **2018**, *781*, 195–200. [[CrossRef](#)]
82. Zadeh, M.A.; Sheykhi, A.; Moradpour, H.; Bamba, K. Note on Tsallis holographic dark energy. *Eur. Phys. J. C* **2018**, *78*, 940. [[CrossRef](#)]
83. Aly, A.A. Tsallis Holographic Dark Energy with Granda-Oliveros Scale in $(-)$ -Dimensional FRW Universe. *Adv. Astron.* **2019**, *2019*, 8138067. [[CrossRef](#)]
84. Srivastava, V.; Sharma, U.K. Tsallis holographic dark energy with hybrid expansion law. *Int. J. Geom. Methods Mod. Phys.* **2020**, *17*, 2050144. [[CrossRef](#)]

85. Sharma, U.K.; Srivastava, V. Tsallis HDE with an IR cutoff as Ricci horizon in a flat FLRW universe. *New Astron.* **2021**, *84*, 101519. [[CrossRef](#)]
86. Nojiri, S.; Odintsov, S.D. The New form of the equation of state for dark energy fluid and accelerating universe. *Phys. Lett. B* **2006**, *639*, 144–150. [[CrossRef](#)]
87. Timoshkin, A.V.; Yurov, A.V. Little Rip, Pseudo Rip and bounce cosmology from generalized equation of state in the universe with spatial curvature. *Int. J. Geom. Meth. Mod. Phys.* **2023**, *20*, 2350204. [[CrossRef](#)]
88. Bento, M.C.; Bertolami, O.; Sen, A.A. Generalized Chaplygin gas, accelerated expansion and dark energy matter unification. *Phys. Rev. D* **2002**, *66*, 043507. [[CrossRef](#)]
89. Nojiri, S.; Odintsov, S.D. DeSitter brane universe induced by phantom and quantum effects. *Phys. Lett. B* **2003**, *565*, 1–9. [[CrossRef](#)]
90. Nojiri, S.; Odintsov, S.D. Quantum de Sitter cosmology and phantom matter. *Phys. Lett. B* **2003**, *562*, 147–152. [[CrossRef](#)]
91. Nojiri, S.; Odintsov, S.D. Quantum escape of sudden future singularity. *Phys. Lett. B* **2004**, *595*, 1–8. [[CrossRef](#)]
92. Nojiri, S.; Odintsov, S.D. The Final state and thermodynamics of dark energy universe. *Phys. Rev. D* **2004**, *70*, 103522. [[CrossRef](#)]
93. Nojiri, S.; Odintsov, S.D. Inhomogeneous equation of state of the universe: Phantom era, future singularity and crossing the phantom barrier. *Phys. Rev. D* **2005**, *72*, 023003. [[CrossRef](#)]
94. Nojiri, S.; Odintsov, S.D. Modified gravity with negative and positive powers of the curvature: Unification of the inflation and of the cosmic acceleration. *Phys. Rev. D* **2003**, *68*, 123512. [[CrossRef](#)]
95. Trivedi, O. Recent advances in cosmological singularities. *arXiv* **2023**, arXiv:2309.08954.
96. de Haro, J.; Nojiri, S.; Odintsov, S.D.; Oikonomou, V.K.; Pan, S. Finite-time cosmological singularities and the possible fate of the Universe. *Phys. Rep.* **2023**, *1034*, 1–114. [[CrossRef](#)]
97. Pasqua, A.; Chattopadhyay, S. A study on the new agegraphic dark energy model in the framework of generalized uncertainty principle for different scale factors. *Int. J. Theor. Phys.* **2014**, *53*, 495–509. [[CrossRef](#)]
98. Myung, Y.S. Instability of holographic dark energy models. *Phys. Lett. B* **2007**, *652*, 223–227. [[CrossRef](#)]
99. Bhattacharjee, S. Interacting Tsallis and Renyi holographic dark energy with hybrid expansion law. *Astrophys. Space Sci.* **2020**, *365*, 103. [[CrossRef](#)]
100. Zubair, M.; Muneer, Q.; Gudekli, E. Thermodynamics and stability analysis of Tsallis Holographic Dark Energy (THDE) models in F (R, T) gravity. *Ann. Phys.* **2022**, *445*, 169068. [[CrossRef](#)]

Disclaimer/Publisher’s Note: The statements, opinions and data contained in all publications are solely those of the individual author(s) and contributor(s) and not of MDPI and/or the editor(s). MDPI and/or the editor(s) disclaim responsibility for any injury to people or property resulting from any ideas, methods, instructions or products referred to in the content.